

Ferroelectric field control of charge density in oxide films with polarization reversal by electric double layer

Ryutaro Nishino^{1,a)}, Yusuke Kozuka¹, Fumitaka Kagawa^{1,2}, Masaki Uchida¹ and Masashi Kawasaki^{1,2}

¹*Department of Applied Physics and Quantum-Phase Electronics Center, University of Tokyo, Bunkyo, Tokyo 113-8656, Japan*

²*RIKEN Center for Emergent Matter Science (CMES), Wako, Saitama 351-0198, Japan*

^{a)}Author to whom correspondence should be addressed. Electronic mail:

nishino@kwsk.t.u-tokyo.ac.jp

Abstract

We demonstrate ferroelectric field control of transport properties in SrRuO₃ and Nb-doped SrTiO₃. We utilize ionic liquid for the polarization reversal of PbZr_{0.2}Ti_{0.8}O₃. The modulation of the sheet resistance in SrRuO₃ is close to the value expected from the polarization-voltage measurement for the PbZr_{0.2}Ti_{0.8}O₃. In the case of Nb-doped SrTiO₃, carrier density for the two polarization states is obtained by the Hall measurement, elucidating modulation of carrier density by $8.0 \times 10^{13} \text{ cm}^{-2}$ at 150 K. These results indicate that polarization reversal via electric double layer can control carrier density of materials beneath the ferroelectric layer similarly to conventional switching techniques utilizing a metal top electrode or a metallic tip of a piezoresponce force microscopy.

Ferroelectric gate field effect transistors (FeFETs), with a channel of conventional semiconductors, have been extensively studied since they have the potential for non-volatility, fast operation and low energy consumption.¹⁻⁴ More recently, ferroelectric gating concept has been extended to control the physical properties of correlated electron oxides that exhibit versatile physical properties such as superconductivity,^{5,6} colossal magneto-resistance⁷ and metal-insulator transition.⁸ In these studies, ferroelectric polarization has been switched by applying a voltage to a counter metal electrode [Fig. 1(a)] or to a metallic tip of a piezoresponce force microscopy (PFM) scanned over the surface of ferroelectric films.

Along with the recent advances of “iontronics”⁹ which investigates controlling electronic properties/functionalities by ionic movement and arrangement, there have been reported examples of polarization reversal in ferroelectric films by the use of the electric double layer (EDL) formed at the interface with ionic liquid (IL) [Fig. 1(b)].¹⁰ When a voltage is applied to a gate electrode immersed in IL, mobile ions in the IL move to the surface of ferroelectric layer to form EDL. To screen the charge of these ions, ferroelectric polarization is stabilized in down (up) state when positive (negative) ions are accumulated on the surface of ferroelectric layer. Compared to the switching techniques utilizing metal counter electrodes in contact with the ferroelectric layer, the use of IL has some advantages. One is feasibility to relatively thin ferroelectric films due to low leakage current through IL. Another is polarization reversal in a large area, which will be useful for some spectroscopic measurements if the IL has reasonable transparency to the probe beam. This technique, for example, has been applied to investigate magnetic depth profile at the interface of ferroelectric $\text{PbZr}_{0.2}\text{Ti}_{0.8}\text{O}_3$ and ferromagnetic $\text{La}_{0.8}\text{Sr}_{0.2}\text{MnO}_3$ by polarized neutron reflectometry measurement, which requires large area samples.¹⁰ In spite of these advantages for exploring ferroelectric field control of electronic properties of oxides, the interaction between ions and ferroelectric surface has not been much investigated. It is not so clear whether employing EDL for the polarization reversal can control the carrier density of the materials beneath the ferroelectric layer similarly to standard switching techniques. Although the use of EDL is not suitable for practical application due to slow ionic motion compared to standard FeFETs^{11,12} with nanosecond order operation, it is important to establish the fundamental device properties for future studies of electric field

effect and iontronics.

Here, we have fabricated devices composed of series connection of EDL and a ferroelectric of $\text{PbZr}_{0.2}\text{Ti}_{0.8}\text{O}_3$ (PZT). We adopted SrRuO_3 and $\text{SrTi}_{0.98}\text{Nb}_{0.02}\text{O}_3$ (Nb-SrTiO₃) as the target materials for the control of charge carrier density because these compounds are most well studied conducting perovskite oxides. SrRuO_3 is a metallic oxide that is often used as electrodes for ferroelectric thin films, exhibiting ferromagnetism below a Curie temperature of 160 K. Nb-SrTiO₃ is a typical n-type oxide semiconductor. Therefore, these two compounds are suitable to examine the modulation of transport properties in our device structure. In the case of the SrRuO_3 , the change in the sheet resistance is in a good agreement with what is expected from polarization (P)-voltage measurement, where carrier density modulation agrees well with the switched polarization, ΔP , (ideally twice the remnant polarization) in the order of $100 \mu\text{C cm}^{-2}$. Therefore, the EDL reversal of ferroelectric polarization is an excellent technique for future studies of electric field effect. In the case of the Nb-SrTiO₃, the modulated carrier density, Δn , is $8.0 \times 10^{13} \text{ cm}^{-2}$ at 150 K, corresponding to $13 \mu\text{C cm}^{-2}$ in ΔP , being much smaller than expected value. However, the value of Δn is comparable to the previous study with ferroelectric field control of Nb-SrTiO₃ that employ a conducting PFM tip⁶, for which possible reasons are discussed.

PZT/ SrRuO_3 and PZT/Nb-SrTiO₃ heterostructures were grown by pulsed laser deposition on SrTiO_3 (001) substrates. The SrRuO_3 (Nb-SrTiO₃) thin films were grown at 700 °C (1100 °C) under 120 mTorr (2×10^{-5} Torr) oxygen pressure. The PZT thin films were then deposited *in situ* on the SrRuO_3 or Nb-SrTiO₃ at 520 °C under 120 mTorr oxygen pressure. For polarization reversal, we employed IL, N,N-diethyl-N-methyl-N-(2-methoxyethyl) ammonium bis (trifluoromethyl-sulfonyl) imide (DEME-TFSI), in which a gate electrode of Pt coil was immersed [Fig. 1 (b)]. The transport properties were measured under vacuum with a back pressure of a 1×10^{-6} Torr. Before the electrical measurement, the IL was stored in a vacuum hot plate at 90 °C for several hours to remove water contamination, which may induce some electrochemical reactions.

We first characterized the ferroelectricity of the PZT thin films. Figure 1(c) shows a PFM image of a PZT film grown on Nb-SrTiO₃. In advance of the measurement,

negative and positive biases were applied while the conductive tip was scanned in the upper and lower rectangle regions, respectively. The phase image indicates that the direction of spontaneous polarization is upward in the as-grown PZT films. Such upward polarization in the as-grown PZT films is also observed elsewhere.¹³ Figure 1(d) shows the polarization-voltage hysteresis loop for a Au/Ni/PZT(300nm)/SrRuO₃(10nm) capacitor structure [Fig. 1(a)]. The remnant polarization and coercive field in this capacitor appear to be $80 \mu\text{C cm}^{-2}$ ($\Delta P = 160 \mu\text{C cm}^{-2}$) and 90 kV/cm , respectively, being similar to those in previous reports.^{14,15} This polarization should induce the modulation of $1.0 \times 10^{15} \text{ cm}^{-2}$ charges, as related by $\Delta P = e\Delta n$, where e is elemental charge.

We then examine the transport properties of SrRuO₃ for the device composed of Pt coil/IL/PZT(25nm)/SrRuO₃(4nm) as shown in Fig. 1(b). In this structure, reciprocal space mapping of x-ray diffraction revealed that the lattices of PZT and SrRuO₃ films are fully strained to match with that of SrTiO₃ substrate. To confirm whether EDL can reverse polarization in a large area, we designed large device area (5 mm length and 2 mm width). We measured sheet resistance (R_s) of SrRuO₃ layer and gate current (I_G) at 260 K as a function of gate voltage (V_G) applied to Pt coil immersed in IL as shown in Fig. 2(b). R_s indicates clear hysteresis similar to polarization-voltage loop. The difference between high and low R_s states at V_G of 0 V preserves $\sim 70\%$ of the initial value for two hours, which will give us enough time for some spectroscopic experiments. Low R_s state at positive V_G (downward polarization state) is consistent with a ferroelectric field effect reported for SrRuO₃.¹⁶ Around the V_G where R_s sharply changes, I_G shows peak structures as denoted by triangles. In a conventional ferroelectric capacitor structure with top and bottom metal electrodes, the displacement current flows with reversal of the polarization direction.¹⁵ In the Pt coil/IL/ferroelectrics/bottom electrode structure, the peaks of I_G should also come from the displacement current. Figure 2(a) is the schematic representations of the polarization reversal of PZT by EDL. At $V_G < 0$ (State A), upward polarization is stabilized. At V_G around coercive voltage (V_C), positive ions accumulated on the PZT surface create downward polarization domain and domain wall (DW) moves to increase downward polarization region (State B). At that time, displacement current flows as I_G . Finally, downward polarization is stabilized in entire region (State C). Since I_G contains not only displacement current (I_{dis}) but also leakage current,¹⁷ we employed a positive-up

negative-down (PUND) method¹⁰ to estimate accurate I_{dis} component, analogous to the ferroelectric polarization measurement. Figure 2(c) shows I_{dis} obtained by the PUND method, where I_G observed for full scan of V_G is subtracted with that for minor loop scans without the polarization reversal [dotted curve in Fig. 2(b)]. To estimate the magnitude of switched polarization ΔP , we integrate I_{dis} by

$$\Delta P = \frac{1}{S} \int I_{\text{dis}} dt \quad (1)$$

as shown in red loop in Fig. 2(c), where S is the sample area. ΔP amounts to $105 \mu\text{C cm}^{-2}$ which is close to that obtained in the conventional ferroelectric capacitor ($\Delta P = 160 \mu\text{C cm}^{-2}$) in Fig. 1(d). In Fig. 2(c), the coercive field in the 25 nm thick PZT appears to be 1000 kV/cm, which is ten times larger than that in the 300 nm thick PZT (Fig. 1(c)). Such enhancement of the coercive field in thin ferroelectric films have been observed elsewhere.¹⁴ Figure 2(d) shows the temperature dependence of R_s for the two polarization state. Ferroelectric field modulates not only R_s but also ferromagnetic transition temperature (T_C) as denoted by triangles, which is determined from the derivation of $R_s - T$ curve. T_C changes from 115 K (upward polarization (P_{up}) state) to 90 K (downward polarization (P_{down}) state). We then roughly estimate the modulated carrier density in SrRuO₃ by the polarization reversal. Assuming the carrier mobility is unchanged for the two polarization states ($\sim 0.8 \text{ cm}^2/\text{Vs}$ (Ref. 18)), the sheet carrier densities at P_{down} and P_{up} states are estimated at $4.4 \times 10^{15} \text{ cm}^{-2}$ and $3.5 \times 10^{15} \text{ cm}^{-2}$ from the R_s modulation, respectively, taking into account the bulk carrier density of SrRuO₃ $\sim 1.0 \times 10^{22} \text{ cm}^{-3}$ (Ref. 18). The modulated carrier density is estimated as $0.9 \times 10^{15} \text{ cm}^{-2}$ and this value corresponds to $140 \mu\text{C cm}^{-2}$ in ΔP , which is in good agreement with ΔP deduced from the device in Fig. 1(a) and 1(b).

Next, we fabricated the device consisting of Pt coil/IL/PZT(40nm)/Nb-SrTiO₃(10nm) as shown in Fig. 1(b). The device length and width are 4 mm and 2 mm, respectively. We also measured carrier density and mobility in the single layer Nb-SrTiO₃ thin films, resulting in $1 \times 10^{20} \text{ cm}^{-3}$ and $40 \text{ cm}^2/\text{Vs}$ at 100 K, respectively. This carrier density corresponds to approximately 30% activation of doped Nb. We then measured the sheet resistance (R_s) of Nb-SrTiO₃ as a function of gate voltage (V_G) at 220 K as shown in Fig. 3(a). R_s clearly shows a hysteresis with a low (high) R_s state when V_G is positive (negative). Since Nb-SrTiO₃ is an n -type semiconductor, R_s

should decrease at P_{down} state (electron accumulation state). Therefore, positive V_G induces downward polarization and accumulates electron carrier, while negative V_G induces upward polarization and depletes carrier. Figure 3(b) shows the temperature dependence of R_s after the polarization is set at P_{down} or P_{up} states. While R_s in P_{down} state preserves metallic conduction down to 2 K, R_s in P_{up} state shows metal-insulator transition around 25 K.

In order to obtain further insight into the difference of transport properties between P_{up} and P_{down} states in Nb-SrTiO₃, we performed Hall effect measurements for each state at several temperatures. Figure 3(e) shows sheet carrier density (n_{2D}) of Nb-SrTiO₃ for each polarization state. From those data, switchable polarization ΔP is estimated as shown in Fig. 3(f) by $\Delta P = e\Delta n_{2D}$, where Δn_{2D} is difference in the carrier density between P_{up} and P_{down} states. Since nonlinear behavior of R_{yx} is observed in P_{down} state below 50 K [Fig. 3(c)] while R_{yx} is linear above 50 K [Fig. 3(d)], we fitted the low temperature data by the two-carrier model assuming low and high mobility electron carriers. As a result of the fitting, the carrier density of low mobility electrons is one or two orders of magnitude higher than that of high mobility electrons. In Fig. 3(e), carrier density at P_{up} state is almost temperature independent but dominant carrier density with low mobility at P_{down} state decreases toward low temperature. Such behavior is observed in electric field induced SrTiO₃ single crystals with a high carrier density $\sim 10^{14} \text{ cm}^{-2}$ (Ref. 19). Consequently, ΔP also decreases toward low temperature. Here, we also plotted previously reported ΔP in the same PZT/Nb-SrTiO₃ (Ref. 6) structure, where polarization of PZT is switched by a conducting PFM tip. ΔP is almost the same value or slightly higher than that of previous study, clearly indicating that polarization reversal by EDL can modulate charge density of materials in contact with ferroelectric layer similarly to standard switching techniques. On the other hand, ΔP deduced by Hall measurement is one order of magnitude smaller than that estimated from polarization-voltage measurement. This result is quite different from the SrRuO₃ case, where the carrier modulation is in the same order with expected value deduced from polarization-voltage measurement. The possible reasons of this discrepancy will be discussed later.

Figure 3(g) shows temperature dependence of the Hall mobility at P_{up} and P_{down} states. At P_{down} state, electron carrier for low (high) mobility is plotted by filled (open)

squares. Mobility at P_{up} state is ten times smaller than that at P_{down} state. This result is in stark contrast with electrostatically doped SrTiO₃ bulk single crystal case where the mobility is almost independent of carrier density.¹⁹ In Nb-SrTiO₃, Nb is known to act not only as donors but also as ionized impurity scatterers at low temperature.²⁰ Impurity concentration in Nb-SrTiO₃ is constant in both polarization states, while the induced carrier density is changed. Therefore, it is natural to consider that large density carriers at P_{down} state can effectively screen random potential of ionized impurities than small density carriers at P_{up} state, resulting in large difference in mobility.

Here, we speculate the reason why the change in carrier density is smaller than that in remnant polarization of PZT deduced from polarization-voltage measurement. One possible origin is defects at the PZT/Nb-SrTiO₃ interface. From the reciprocal space mapping measurement, we find that Nb-SrTiO₃ is coherently grown to SrTiO₃ substrate, but PZT is completely relaxed, inducing misfit dislocations at the PZT/Nb-SrTiO₃ interface. Accumulated carriers may tend to be trapped at the PZT/Nb-SrTiO₃ interface, resulting in no contribution to the Hall effect. Another possible origin is polar distortion of SrTiO₃. Quantum paraelectric SrTiO₃ is easily turned into ferroelectric state by electric field²¹ or strain.²² In fact, ferroelectric distortion of SrTiO₃ has been observed at the LaAlO₃/SrTiO₃ interface.²³ Also ferroelectric polarization of SrTiO₃ is theoretically predicted at the PbTiO₃/SrTiO₃ interface²⁴ and experimentally confirmed at BaTiO₃/SrTiO₃ superlattice.²⁵ Under such conditions, PZT polarization at the interface is screened by the spontaneous polarization in SrTiO₃ rather than carrier accumulation. These points need to be cleared in future study.

In conclusion, we have fabricated the devices employing EDL for the polarization reversal of ferroelectric layer. We have shown that this structure can control transport properties of materials beneath the ferroelectric layer

similarly to standard switching techniques. In the case for SrRuO₃, carrier density is modulated as expected from polarization-voltage measurement. In the case for Nb-SrTiO₃, carrier modulation shows similar or slightly higher values compared to the previous study utilizing standard switching techniques, although this value is smaller than expected value from PZT remnant polarization unlike the SrRuO₃ case. We clearly demonstrate that polarization reversal via EDL can be applied for ferroelectric control of physical properties

of oxide materials, providing an approach for investigating the electronic properties/functionalities in the ions/ferroelectrics and ferroelectrics/oxides interfaces.

This work was partly supported by the Japan Science and Technology Agency Core Research for Evolutional Science Technology (JST CREST) (No. JPMJCR16F1).

References

- ¹ J. Hoffman, X. Pan, J.W. Reiner, F.J. Walker, J.P. Han, C.H. Ahn, and T.P. Ma, *Adv. Mater.* **22**, 2957 (2010).
- ² S.L. Miller and P.J. McWhorter, *J. Appl. Phys.* **72**, 5999 (1992).
- ³ S. Mathews, R. Ramesh, T. Venkatesan, and J. Benedetto, *Science* **276**, 238 (1997).
- ⁴ R.C.G. Naber, C. Tanase, P.W.M. Blom, G.H. Gelinck, A.W. Marsman, F.J. Touwslager, S. Setayesh, and D.M. De Leeuw, *Nat. Mater.* **4**, 243 (2005).
- ⁵ C.H. Ahn, S. Gariglio, P. Paruch, T. Tybell, L. Antognazza, and J.-M. Triscone, *Science* **284**, 1152 (1999).
- ⁶ K.S. Takahashi, M. Gabay, D. Jaccard, K. Shibuya, T. Ohnishi, M. Lippmaa, and J.-M. Triscone, *Nature* **441**, 195 (2006).
- ⁷ B. Cui, C. Song, H. Mao, H. Wu, F. Li, J. Peng, G. Wang, F. Zeng, and F. Pan, *Adv. Mater.* **27**, 6651 (2015).
- ⁸ L. Zhang, X.G. Chen, H.J. Gardner, M.A. Koten, J.E. Shield, and X. Hong, *Appl. Phys. Lett.* **107**, 152906 (2015).
- ⁹ S.Z. Bisri, S. Shimizu, M. Nakano, and Y. Iwasa, *Adv. Mater.* **29**, 1607054 (2017).
- ¹⁰ A. Herklotz, E.J. Guo, A.T. Wong, T.L. Meyer, S. Dai, T.Z. Ward, H.N. Lee, and M.R. Fitzsimmons, *Nano Lett.* **17**, 1665 (2017).
- ¹¹ N. Gong and T.P. Ma, *IEEE Electron Device Lett.* **39**, 15 (2018).
- ¹² N. Gong and T.P. Ma, *IEEE Electron Device Lett.* **37**, 1123 (2016).
- ¹³ V. Nagarajan, J. Junquera, J.Q. He, C.L. Jia, R. Waser, K. Lee, Y.K. Kim, S. Baik, T.

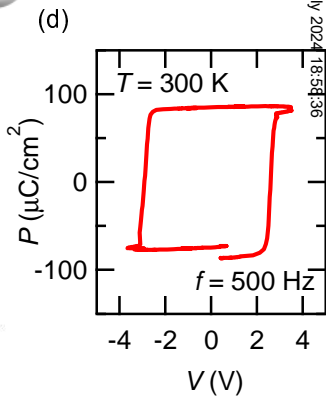
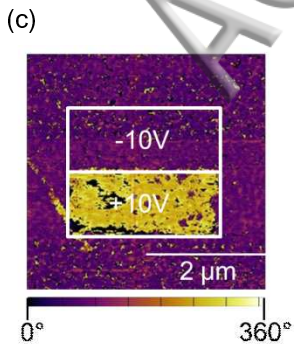
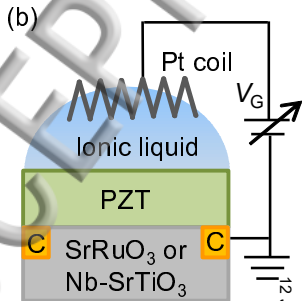
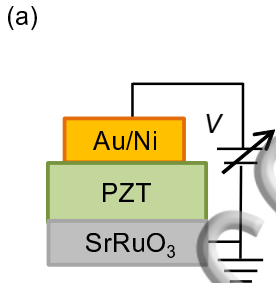
- Zhao, R. Ramesh, Ph. Ghosez, and K.M. Rabe, *J. Appl. Phys.* **100**, 051609 (2006).
- ¹⁴ V. Nagarajan, S. Prasertchoung, T. Zhao, H. Zheng, J. Ouyang, R. Ramesh, W. Tian, X.Q. Pan, D.M. Kim, C.B. Eom, H. Kohlstedt, and R. Waser, *Appl. Phys. Lett.* **84**, 5225 (2004).
- ¹⁵ I. Vrejoiu, G. Le Rhun, L. Pintilie, D. Hesse, M. Alexe, and U. Gösele, *Adv. Mater.* **18**, 1657 (2006).
- ¹⁶ C.H. Ahn, R.H. Hammond, T.H. Geballe, M.R. Beasley, J.-M. Triscone, M. Decroux, O. Fischer, L. Antognazza, and K. Char, *Appl. Phys. Lett.* **70**, 206 (1997).
- ¹⁷ H. Yuan, H. Shimotani, J. Ye, S. Yoon, H. Aliah, A. Tsukazaki, M. Kawasaki, and Y. Iwasa, *J. Am. Chem. Soc.* **132**, 18402 (2010).
- ¹⁸ Y. Ohuchi, J. Matsuno, N. Ogawa, Y. Kozuka, M. Uchida, Y. Tokura, and M. Kawasaki, *Nat. Commun.* **9**, 213 (2018).
- ¹⁹ K. Ueno, S. Nakamura, H. Shimotani, A. Ohtomo, N. Kimura, T. Nojima, H. Aoki, Y. Iwasa, and M. Kawasaki, *Nat. Mater.* **7**, 855 (2008).
- ²⁰ O.N. Tufte and P.W. Chapman, *Phys. Rev.* **155**, 796 (1967).
- ²¹ M.A. Saifi and L.E. Cross, *Phys. Rev. B* **2**, 677 (1970).
- ²² J.H. Haeni, P. Irvin, W. Chang, R. Uecker, P. Reiche, Y.L. Li, S. Choudhury, W. Tian, M.E. Hawley, B. Craigo, A.K. Tagantsev, X.Q. Pan, S.K. Streiffer, L.Q. Chen, S.W. Kirchoefer, J. Levy, and D.G. Schlom, *Nature* **430**, 758 (2004).
- ²³ C.L. Jia, S.B. Mi, M. Faley, U. Poppe, J. Schubert, and K. Urban, *Phys. Rev. B* **79**, 081405 (2009).
- ²⁴ M. Sepiarsky, M.G. Stachiotti, and R.L. Migoni, *Phys. Rev. Lett.* **96**, 137603 (2006).
- ²⁵ D.A. Temme, A. Bruchhausen, N.D. Lanzillotti-Kimura, A. Fainstein, R.S. Katiyar, A. Cantarero, A. Soukiassian, V. Vaithyanathan, J.H. Haeni, W. Tian, D.G. Schlom, K.J. Choi, D.M. Kim, C.B. Eom, H.P. Sun, X.Q. Pan, Y.L. Li, L.Q. Chen, Q.X. Jia, S.M. Nakhmanson, K.M. Rabe, and X.X. Xi, *Science* **313**, 1614 (2006).

Figure Captions

Fig. 1. Capacitor structures with (a) conventional metal top electrode and (b) Pt coil/ionic liquid hybrid top electrode. C stands for contact electrodes for resistivity measurement. (c) The phase contrast image of a PZT thin film on Nb-SrTiO₃ measured by piezoresponce force microscopy. Before measurement, negative (-10 V) and positive (+10 V) biases are applied in upper and lower rectangle regions, respectively. (d) Polarization (P) voltage (V) loop measured at 500 Hz and 300 K for device (a) with 300 nm thick PZT film.

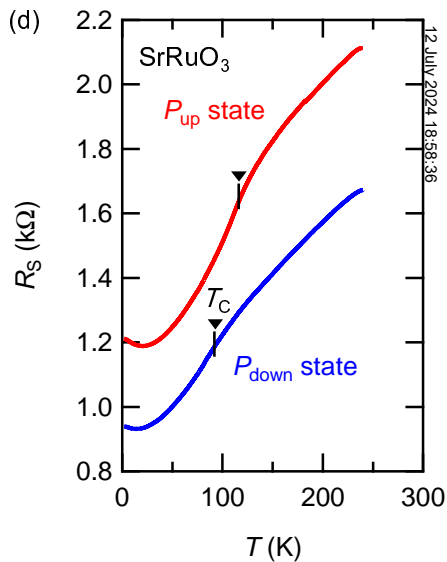
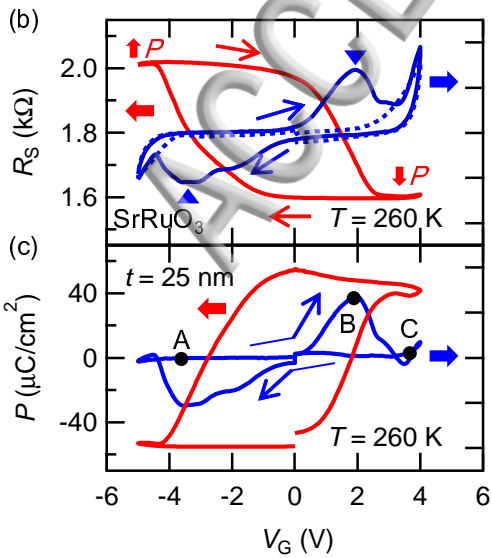
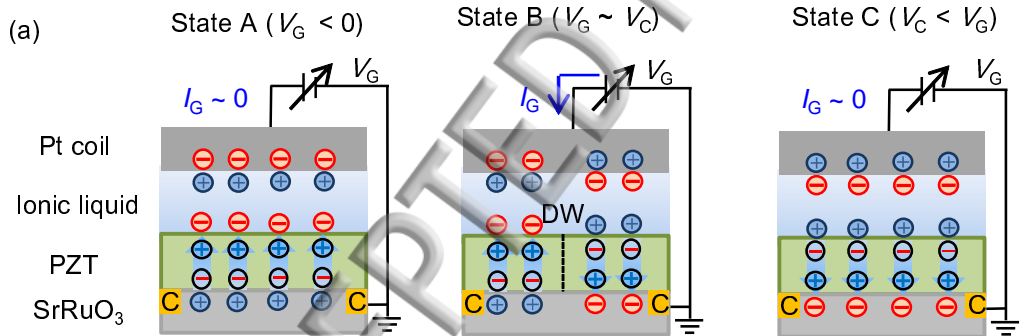
Fig. 2. (a) Schematic representation of the polarization reversal in ferroelectric PZT film while gate voltage (V_G) is scanned from negatively saturated (State A) through positive coercive voltage V_C (State B) to positively saturated (State C) states. Broken line in middle panel stands for domain wall (DW). (b) Sheet resistance (R_s (red)) and gate current (I_G (blue solid curve)) at 260 K measured while V_G is scanned at 50 mV/s. Dotted blue curve is the leakage current deduced by a positive-up negative-down (PUND) method. (c) Displacement current (I_{dis} (blue)) and polarization (red) deduced by the PUND method from the data in (b). Arrows indicate the scan directions. (d) Sheet resistance (R_s) of the SrRuO₃ in respective polarization states of PZT. Triangles indicate ferromagnetic transition temperature (T_C) of SrRuO₃ determined from derivation of $R_s - T$ curve.

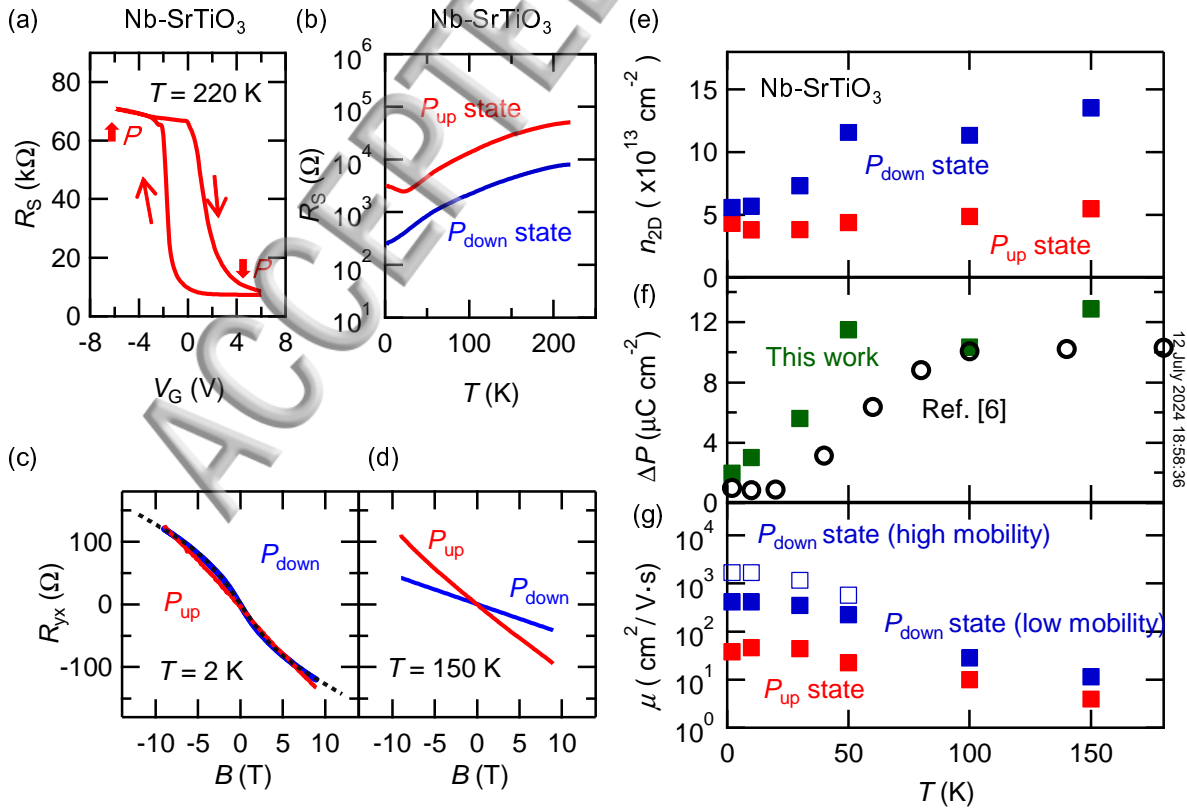
Fig. 3. (a) Sheet resistance (R_s) of Nb-SrTiO₃ at 220 K as a function of gate voltage (V_G) scanned at 100 mV/s. (b) Temperature dependence of R_s for the P_{up} (red) and P_{down} (blue) states of PZT. Hall resistance of Nb-SrTiO₃ for the P_{up} (red) and P_{down} (blue) states of PZT at (c) 2 K and (d) 150 K. The dotted curve is the fitted function. (e) Sheet carrier density of Nb-SrTiO₃ for the two polarization states of PZT at various temperatures. (f) Switched polarization ΔP calculated from Δn_{2D} in (e) at various temperatures. Open circles are adapted with permission from Reference 6; copyright 2006, Nature Publishing Group. (g) Polarization-dependence of Hall mobility (μ) as a function of temperature.



12 July 2024

18:58:36





12 July 2024 18:58:36